Available online at www.sciencedirect.com
SCIENCE DIRECT®
Journal of Solid State Chemistry 177 (2004) 73–79
JOURNAL OF SOLID STATE CHEMISTRY
http://elsevier.com/locate/jssc

Synthesis and magnetic properties of the quasi-one-dimensional compound $Ca_{0.83}(Cu_{1-x}Co_x)O_2$

Yuzuru Miyazaki*

Department of Applied Physics, Graduate School of Engineering, Tohoku University, Aramaki Aoba, Aoba-ku, Sendai 980-8579, Japan

Received 20 February 2003; received in revised form 19 May 2003; accepted 30 May 2003

Abstract

A new solid solution of the quasi-one-dimensional composite crystal, $Ca_{0.83}(Cu_{1-x}Co_x)O_2$ $(0 \leqslant x \leqslant 0.30)$, has been synthesized under 1 atm of O_2 at 830°C. The non-doped compound $Ca_{0.83}CuO_2$ consists of two interpenetrating monoclinic subsystems of the [Ca] atoms and the edge-shared square planar $[CuO_2]$ chains. Upon increasing x, both the subsystems undergo a phase change from monoclinic to orthorhombic $(M-O)$. The $M-O$ change occurs at $x \sim 0.04$ for the $[(Cu, Co)O_2]$ subsystem, while such a change occurs at $x \sim 0.17$ for the [Ca] subsystem. Magnetic susceptibility measurements show an evolution from a short-range ordered state near $x = 0$ to a long-range antiferromagnetic state ($T_N = 10-15$ K) for the samples with $x \geqslant 0.15$. The effective magnetic moment μ_{eff} is found to increase with increasing x from 2.1 μ_B for $x = 0.10$ to 3.0 μ_B for $x = 0.30$, suggesting that the solid solution can be regarded as $Ca_{0.83}[Cu^{2+}_{0.66}Cu^{3+}_{0.34-x}Co^{3+}_x]O_2$, in which a mixed state of $Cu^{2+}(S = 1/2)$, $Cu^{3+}(S = 0)$ and high-spin $Co^{3+}(S = 2)$ ions is realized.

Keywords: Low-dimensional compound; Composite crystal; Magnetic susceptibility; Calcium cobalt copper oxide; Substitution effects

1. Introduction

Quasi-one-dimensional (1D) cuprate $(Ca_{1-x}Y_x)_y CuO_2$ $(y \sim 0.83)$ has recently attracted much attention owing to its unique structure [1–8] and magnetic properties [8–13]. Miyazaki et al., [5,6] have successfully determined the modulated crystal structure of the solid solution by a superspace group approach. Isobe et al., [8] have independently determined the crystal structure of a terminal compound and obtained results similar to Ref. [6]. Both authors have described that the compound is built up from two interpenetrating subsystems as shown in Fig. 1. Subsystem 1 consists of 1D $[CuO_2]$ chains with sharing opposite edges of CuO_4 squares, while subsystem 2 comprises $[Ca_{1-x}Y_x]$ layers interleaving the $[CuO_2]$ chains. Since both subsystems have mutually incommensurate periods parallel to the a-axis, the compositional parameter y usually yields an incommensurate value between 0.81 and 0.84, depending on x. Due to this change, the formal valence state of Cu (Cu^{p+}) varies from $p = 2.00$ to 2.34. The magnetic behavior of the compound is largely affected by the Cu valence, evolving from a three-dimensional (3D) antiferromagnetic (AF) state to a 1D AF state. The sample with $x = 0.435$ $(p = 2.00)$ exhibits a paramagnetic to AF transition at $T_N = 29$ K, while the sample with $x = 0$ $(p = 2.34)$ shows a broad maximum at 30 K in the magnetic susceptibility curve [10,11]. With decreasing x (equivalent to increase in p value), T_N decreases gradually and eventually disappears at around $x = 0.20$ $(p = 2.20)$, followed by emergence of the 1D state. Extensive studies have been performed to investigate the physical properties of the solid solution as a diluted $S = 1/2$ magnetic system, revealing that the system can be well described as a mixture of Curie–Weiss, spin dimers and/or alternating Heisenberg chain components [7,12,13]. In the 1D region, most of the doped holes (Cu^{3+}) are believed to form non-magnetic $(S = 0)$ Zhang–Rice singlets [14] and to localize at low temperatures, leading to the dilution of long-range spin correlations. Hence, the Zhang–Rice singlets "◦" are mediated by $S = 1/2$ spins (up and down spins as "↑" and "↓") and situated almost every third Cu sites as "↓◦↑↑◦↓…" [8,12]. Next our interest is in the question how the magnetic behavior evolves when a part of

*Fax: +81-22-217-7982.
E-mail address: miya@crystal.apph.tohoku.ac.jp.

0022-4596/03/$ - see front matter © 2003 Elsevier Inc. All rights reserved.
doi:10.1016/S0022-4596(03)00312-8

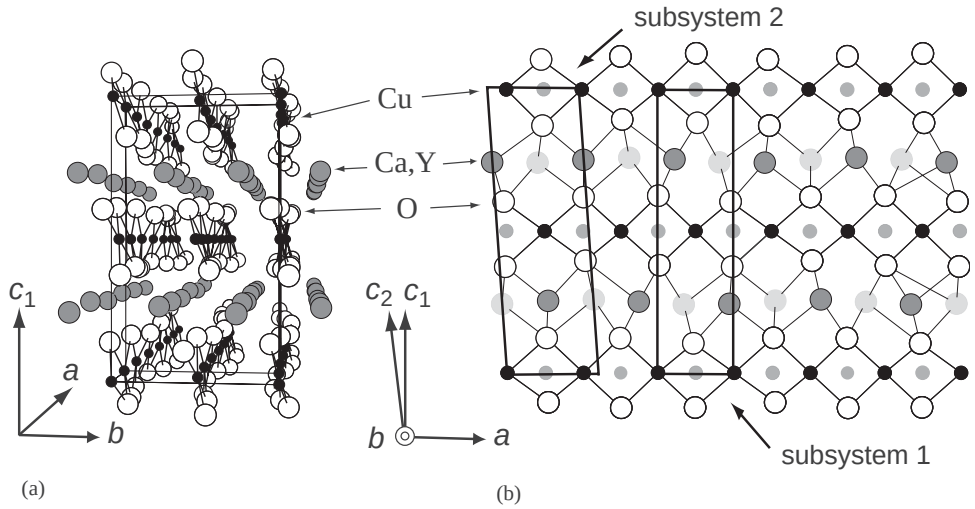

Fig. 1. The composite crystal structure of $(Ca_{1-x}Y_x)_yCuO_2$ viewed in perspective from the *a*-axis (a) and parallel to the *b*-axis (b) (Ref. [6]).

Zhang–Rice singlet sites are substituted by other trivalent ions with a different spin quantum number. Among a number of ions, Co^{3+} appears to have the largest solubility in the Cu ions with square-planer coordination, as reported in $YBa_2Cu_3O_7$ [15] and in $(Sr,Ca)_{14}Cu_{24}O_{41}$ [16]. We have then discovered that the Cu ions can be substituted up to $\sim 30\%$ by the Co ions in the present compound, without any noticeable change in oxygen content. In this report, we present conjoint crystal structure analyses and magnetic susceptibility of $Ca_{0.83}(Cu_{1-x}Co_x)O_2$ with $0 \leqslant x \leqslant 0.30$. Experimental data strongly suggest that the doped Co ions are in a high-spin ($S = 2$) state and dominantly substitute for the trivalent Cu ions.

2. Experimental

Polycrystalline samples were prepared by the standard solid-state reaction method. Appropriate amounts of $CaCO_3$ (99.9%), CuO (99.99%) and Co_3O_4 (99.995%) powders were mixed with an agate mortar and pressed into pellets. The pellets were heated at 830°C for 20 h in flowing oxygen gas. Then, the samples were furnace cooled to room temperature, ground and pelletized again. This sintering process was repeated until the homogeneous samples were obtained.

X-ray diffraction (XRD) data were collected with Cu$K\alpha$ radiation at room temperature in the 2θ range of 10–100° with 0.040° step using a Rigaku RAD-X diffractometer equipped with a curved graphite monochromator. The XRD data were analyzed using a Rietveld refinement program PREMOS 91 [17], designed for modulated structure analyses. Magnetic susceptibility of the powdered samples was measured using a superconducting quantum interference device (SQUID) magnetometer (Quantum Design MPMS-5HR) from 300 to 4 K with zero-field cooling (ZFC) and field cooling (FC) conditions under the magnetic field of $H = 1000$ Oe.

3. Results and discussion

3.1. Synthesis and crystal structure

Fig. 2 shows the XRD patterns ($2\theta = 25-45°$) of the samples with nominal composition of $Ca_{0.83}(Cu_{1-x}Co_x)O_2$ at room temperature. Four integers, *h k l m*, are necessary to index the Bragg peaks, including satellite reflections originating from the interaction between the subsystems. We assigned the $(Cu,Co)O_2$ chains to subsystem 1 and the Ca atoms to subsystem 2. For example, the peaks denoted as "*h k l* 0" and "0 *k l m*" are, respectively, originating from fundamental reflections of the subsystems 1 and 2, while the peaks of "*h k l m*" are satellite ones. Both the subsystems are monoclinic for the non-doped compound $Ca_{0.83}CuO_2$, with $\beta_1 = 90.08(1)°$ and $\beta_2 = 93.04(1)°$ (as shown in Table 1). One may easily recognize that two sets of reflections belonging to the subsystem 2, "0 *k l m*" and "0 *k l m*", become close to each other with increasing *x* and then overlap at around $x = 0.15$, implying that the monoclinic subsystem changes to the orthorhombic one. The single-phase samples are obtained for the compositional parameter *x* with $0 \leqslant x \leqslant 0.30$. The second phase $Ca_3Co_2O_6$ (shown as asterisks) is found to appear for the samples with $x \geqslant 0.35$. Since our preliminary thermogravimetric analysis (TGA) revealed no detectable oxygen offstoichiometry from 2.00 for all the single-phase samples, the mixed-valent $(Cu,Co)^{p+}$ site must have a nominal valence of $p \sim 2.34$ over the entire range of *x* due to the charge neutrality. In an oxidizing atmosphere, the

Cu ions prefer the oxidation states of 2+ and 3+, while the Co ions favor the valences with 3+ and 4+. If the tetravalent Co ions substitute for the Cu ions, a part of Cu^{3+} must be reduced to the Cu^{2+} state to maintain the total (Cu, Co) valence state as 2.34. For this mixed-valence state, the solubility limit would be $x \sim 0.2$. On the basis of the fact that the solubility limit of Co is around $x = 0.30$ as shown in Fig. 2, the Co ions should take a trivalent state and mainly substitute for the trivalent Cu ions. Then, the solid solution can be regarded as $Ca_{0.83}[Cu^{2+}_{0.66}Cu^{3+}_{0.34-x}Co^{3+}_{x}]O_2$.

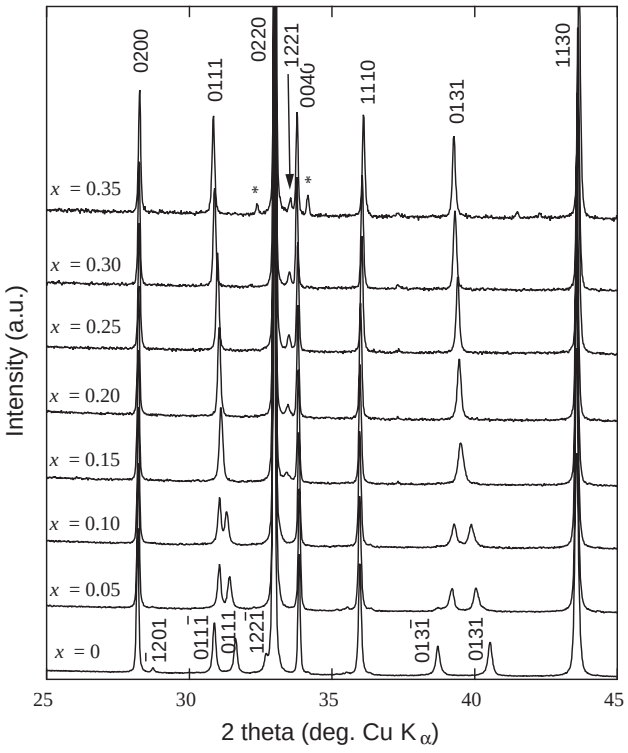

Fig. 2. Powder XRD patterns of the $Ca_{0.83}(Cu_{1-x}Co_x)O_2$ solid solution. The integers denoted "$h\ k\ l\ 0$" and "$0\ k\ l\ m$" are, respectively, originated from fundamental reflections of the $[(Cu, Co)O_2]$ subsystem and [Ca] subsystem, and the peaks of "$h\ k\ l\ m$" are satellite ones.

In order to obtain more detailed structural information, we performed Rietveld analysis for the powdered samples. Due to the difficulty in refining complete modulation from XRD data alone, the modulation amplitudes of the atoms were adopted from the previous structure data of the end-member, $Ca_{0.83}CuO_2$ [6]. Satisfactorily low R-values (<10%) were obtained for all the samples. Fig. 3 shows the refined lattice parameters plotted against x. The refined lattice parameters and the modulation vector elements along the a^*- and c^*-axis, α and γ, are summarized in Table 1. Numbers in parentheses represent estimated standard deviations of the last significant digits. The c_2-axis length can be obtained from the equation $c_1 \sin\beta_1 = c_2 \sin\beta_2$. Note that the γ value equals to 0 when the subsystem 2 becomes orthorhombic. Each panel in Fig. 3 can be divided into three regions according to the symmetry of the subsystems. Both subsystems are monoclinic in the lower Co-doped region of $x < 0.05$("$M^1 + M^2$"). Subsystem 1 becomes orthorhombic while subsystem 2 remains monoclinic in the range with $0.05 \leqslant x \leqslant 0.16$("$O^1 + M^2$"). With further increase in x, subsystem 2 also becomes orthorhombic ("$O^1 + O^2$"). All the lattice parameter values show continuous change with increasing x. The a_1-axis length slightly increases and then turns to decrease around the "$M^1 + M^2$" and "$O^1 + M^2$" boundary, while the a_2-axis length shows a reverse tendency. The magnitude of the change (between $x = 0$ and $x = 0.30$) is much significant in the a_2-axis, i.e., $\Delta a_2 \sim 0.05$ Å (1.5%) being larger than that of a_1-axis, $\Delta a_1 \sim 0.01$ Å (0.3%). Contrary to the a-axis lengths, the b-axis length exhibits a sudden decrease at around $x = 0.10$ and then approaches a constant value (6.305 Å) with further

Table 1
Refined structural parameters of $Ca_{0.83}(Cu_{1-x}Co_x)O_2$

x	a_1 (Å)	a_2 (Å)	b (Å)	c_1 (Å)	β_1 (deg)	β_2 (deg)	α	γ
0	2.8063(2)	3.3645(2)	6.3197(4)	10.5751(7)	90.08(1)	93.04(1)	0.8341(2)	0.1591(14)
0.03	2.8079(2)	3.3639(2)	6.3185(4)	10.5751(6)	90.02(1)	91.72(1)	0.8347(2)	0.0974(12)
0.05	2.8082(2)	3.3635(2)	6.3172(5)	10.5749(8)	90	91.40(1)	0.8349(2)	0.0769(10)
0.10	2.8076(1)	3.3721(1)	6.3155(3)	10.5770(6)	90	90.97(1)	0.8326(2)	0.0530(10)
0.11	2.8070(2)	3.3724(2)	6.3139(4)	10.5772(6)	90	90.84(1)	0.8323(1)	0.0462(8)
0.12	2.8057(2)	3.3720(2)	6.3119(4)	10.5766(7)	90	90.76(1)	0.8321(2)	0.0416(9)
0.13	2.8058(2)	3.3752(2)	6.3117(4)	10.5771(6)	90	90.60(1)	0.8313(2)	0.0325(8)
0.14	2.8045(2)	3.3766(2)	6.3100(5)	10.5782(8)	90	90.46(1)	0.8306(2)	0.0253(11)
0.15	2.8043(1)	3.3795(1)	6.3098(5)	10.5775(4)	90	90.24(1)	0.8298(2)	0.0133(8)
0.16	2.8040(2)	3.3803(2)	6.3095(4)	10.5789(4)	90	90.08(1)	0.8291(1)	0.0088(10)
0.18	2.8033(2)	3.3832(2)	6.3089(4)	10.5791(6)	90	90	0.8288(2)	0
0.20	2.8019(2)	3.3893(2)	6.3067(5)	10.5813(8)	90	90	0.8267(2)	0
0.25	2.8008(1)	3.4023(1)	6.3088(2)	10.5911(4)	90	90	0.8232(1)	0
0.30	2.7977(1)	3.4160(1)	6.3062(3)	10.5953(4)	90	90	0.8190(1)	0

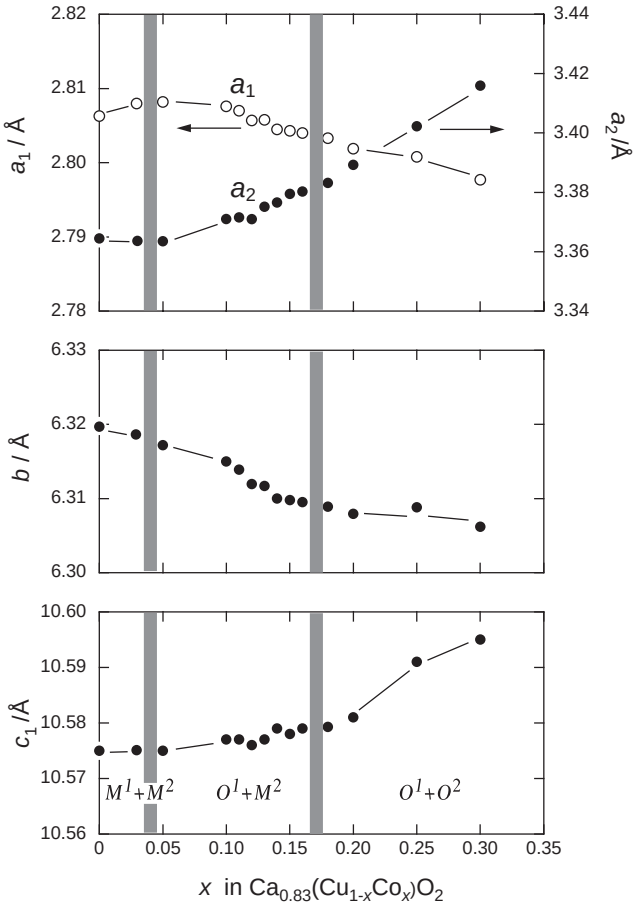

Fig. 3. Effect of cobalt substitution on the lattice parameters of $Ca_{0.83}(Cu_{1-x}Co_x)O_2$ solid solution. The letters M and O represent "monoclinic" and "orthorhombic", and superscripts "1" and "2" corresponds to the subsystems 1 and 2, respectively. Two thick lines in each panel are determined phase boundaries between $M^1 + M^2$ and $O^1 + M^2$, $O^1 + M^2$ and $O^1 + O^2$.

increase in x. The c_1-axis length starts to increase markedly in the range $x > 0.20$. As demonstrated by Miyazaki et al., [5,6], the $a_1/a_2(\equiv \alpha)$ ratio represents the relative Ca content of the present samples, $Ca_\alpha(Cu, Co)O_2$. The α values shown in Table 1 tend to decrease gradually with the increase of x, even though all the samples were prepared with a nominal composition of $Ca_{0.83}$ (Cu, Co) O_2.

With regard to the coordination geometry, both the Cu and Co ions could have a tetrahedral coordination of the O ions. The Cu^{2+} and Cu^{3+} ions are known to prefer a square planer coordination while the Co^{3+} ion favors a regular tetrahedral coordination. Thus, one may expect that the substitution of Co for Cu would lead to the systematic change from the square-type (Cu, Co) O_2 coordination to the distorted tetrahedral-type one. If such a picture is realized, the b-axis length and the c-axis length should, respectively, increase and decrease with x. However, the observed change in the lattice parameters contradicts this assumption. To rationalize the observation, each O site must shift cooperatively so as to contract the CaO_6 octahedra parallel to the c-axis and elongate them in the a-axis.

3.2. Magnetic properties

Fig. 4 shows the temperature dependence of the magnetic susceptibility, $\chi(T)$, of $Ca_{0.83}$ $(Cu_{1-x}Co_x)$ O_2 solid solution measured under the FC condition. As reported in preceding papers [7,9,10,12], the Co-free $Ca_{0.83}CuO_2$ samples show a broad maximum at around 30 K in the $\chi(T)$ curve, characteristic of a 1D AF system, followed by a Curie–Weiss upturn at lower temperature. Partial substitution of Co ions for the Cu ions is found to increase absolute $\chi(T)$ values over the whole temperature range below 300 K. With increasing x, paramagnetic contribution is enhanced and the broad maximum temperature lowers from ~ 30 K $(x = 0)$ to ~ 15 K $(x = 0.10)$. The samples with $x \geqslant 0.15$ show small but distinct long-range AF order at low temperatures, varying gradually from $T_N = 10$ K $(x = 0.15)$ to 15 K $(x = 0.30)$. No detectable difference in the $\chi(T)$ curve was observed between the ZFC and FC conditions for each sample.

To examine whether the samples follow the Curie–Weiss law, the inverse susceptibility (χ^{-1}) versus temperature curves are plotted in the inset of Fig. 4. To avoid overlapping of the data points, the $x = 0.15$ and 0.25 data are not shown in the inset. For the samples with $x \geqslant 0.10$, $\chi^{-1}(T)$ is found to obey the Curie–Weiss law above 50 K. The effective magnetic moment μ_{eff} was then determined using the obtained

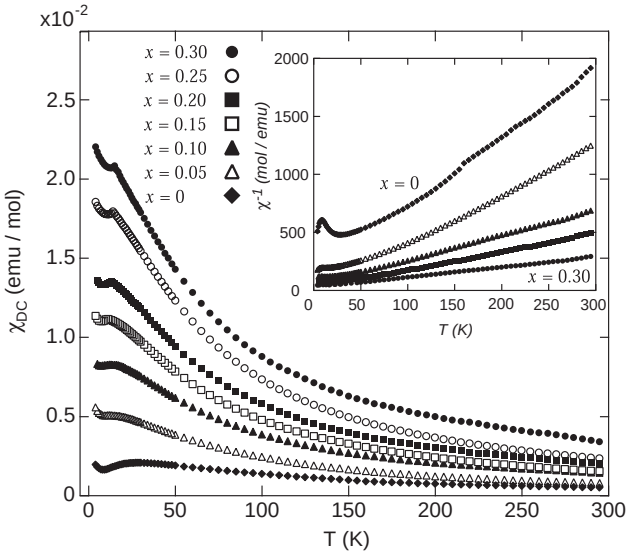

Fig. 4. Temperature dependence of the magnetic susceptibility under the applied magnetic field of 1000 Oe for $Ca_{0.83}(Cu_{1-x}Co_x)O_2$. The inverse susceptibility is plotted in the inset. To avoid the overlapping of the data points, the $x = 0.15$ and 0.25 data are not shown in the inset.

Table 2
Determined values of the Weiss temperature θ and the effective magnetic moment μ_{eff} of $Ca_{0.83}(Cu_{1-x}Co_x)O_2$ together with the calculated μ_{calc} values

x	θ(K)	C (emu K/mol)	μ_{eff} (μ_B)	μ_{calc} (μ_B)
0.10	−33.6(9)	0.542(11)	2.08(3)	2.1
0.15	−37.9(8)	0.766(8)	2.48(3)	2.4
0.20	−32.0(10)	0.831(13)	2.58(4)	2.6
0.25	−31.3(9)	1.07(1)	2.93(2)	2.8
0.30	−28.1(8)	1.12(1)	2.99(2)	3.0

Curie constant C and the equation $\mu_{eff} = [3k_BC/(N\mu_B^2)]^{1/2}$, where k_B, N and μ_B are the Boltzmann's constant, the Avogadro's number and the Bohr magneton, respectively. Table 2 summarizes the obtained parameters together with the calculated effective magnetic moment μ_{calc} described below. For all the samples, the Weiss temperature θ is negative and around −30 K, implying a weak AF interaction between the magnetic spins. As expected from the slope of $\chi^{-1}(T)$ curve, μ_{eff} value gradually increases with x from 2.08(3) μ_B ($x = 0.10$) to 2.99(2) μ_B ($x = 0.30$). Considering a square-planar $(Cu, Co)O_2$ coordination (D_{4h} point group), the crystal field splitting of d orbitals yields the following energy order; $e_g(d_{xz}, d_{yz}) < a_{1g}(d_{3z^2-r^2}) < b_{2g}(d_{xy}) < b_{1g}(d_{x^2-y^2})$ [18]. Although significant modulation of the O atom sites would cause some modification on the energy-level splittings, the deviations of the diagonal O–Cu–O angles are estimated to be $180 \pm 25°$ from the structure data of $Ca_{0.83}CuO_2$ [6] and therefore, the order of energy levels should remain unchanged. Under such a "quasi" square-planar ligand field, the electronic configuration of Cu^{2+} ions is written as $e_g^4 a_{1g}^2 b_{2g}^2 b_{1g}^1$ ($S = 1/2$). The Cu^{3+} ($3d^8$) ions could take either a high-spin ($e_g^4 a_{1g}^2 b_{2g}^1 b_{1g}^1 : S = 1$) or a low-spin ($e_g^4 a_{1g}^2 b_{2g}^2 b_{1g}^0 : S = 0$) state. Similarly, the Co^{3+} ($3d^6$) ions would take one of the possible three states; high spin ($e_g^{2+1} a_{1g}^1 b_{2g}^1 b_{1g}^1 : S = 2$), intermediate spin ($e_g^4 a_{1g}^1 b_{2g}^1 b_{1g}^0 : S = 1$) or low spin ($e_g^4 a_{1g}^2 b_{2g}^0 b_{1g}^0 : S = 0$). To evaluate a possible spin state for the magnetic ions, the effective magnetic moment, μ_{calc}, was calculated using the formula; $\mu_{calc} = g\sqrt{\sum_i [N_i S_i(S_i+1)]}$, where $g = 2.0$, and N_i and S_i ($i = 1, 2, 3$) denote the molar ratio and spin quantum number for the ith magnetic ions (i.e., Cu^{2+}, Cu^{3+} and Co^{3+}), respectively. Since the solid solution system is represented as $Ca_{0.83}[Cu^{2+}_{0.66}Cu^{3+}_{0.34-x}Co^{3+}_x]O_2$, the above formula is modified as

$$\mu_{calc} = 2\sqrt{0.66 \times 3/4 + (0.34 - x) \times S_{Cu^{3+}}(S_{Cu^{3+}} + 1) + x \times S_{Co^{3+}}(S_{Co^{3+}} + 1)}.$$

Among the possible electronic configurations, the combination of $Cu^{3+}(S = 0)$ and $Co^{3+}(S = 2)$ gives quite good agreement with the observed μ_{eff} and calculated μ_{calc} values as shown in Table 2. Of course, the orbital contribution should not be negligible for such a $Co^{3+}(d^6)$ ion and it would be taken into account for further quantitative discussion. From the electric resistivity measurements, all the samples were found to be highly insulating with resistivities $\rho > 10^5$ Ω cm at room temperature. Therefore, charge transfer between the magnetic sites is extremely small and the solid solution can be regarded as a localized spin system where high-spin ($S = 2$) Co^{3+} ions most dominantly substitute for the low-spin ($S = 0$) Cu^{3+} ions.

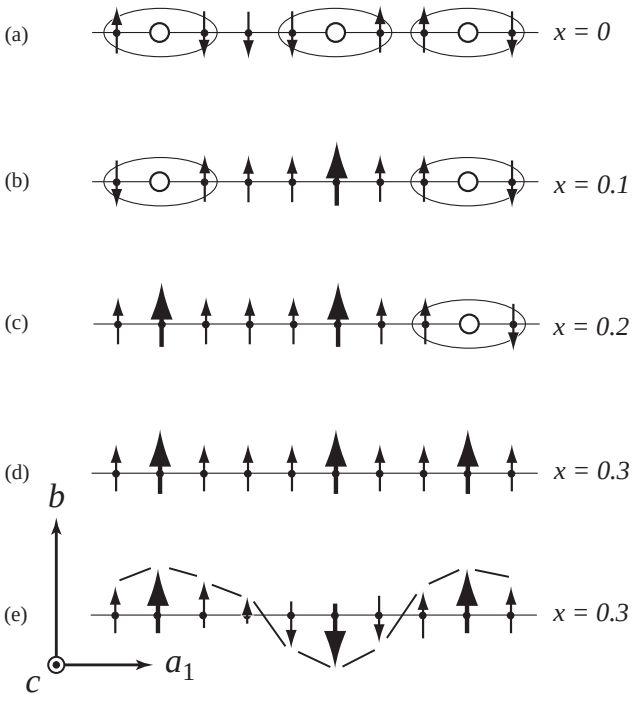

Fig. 5. Schematic representation of possible spin configurations on a magnetic chain (ten sites) upon doping for $Ca_{0.83}(Cu_{1-x}Co_x)O_2$. Small and large arrows represent $Cu^{2+}(S = 1/2)$ and $Co^{3+}(S = 2)$ spins, respectively. The Cu^{3+} spins form so-called Zhang–Rice singlets, depicted as small open circles.

Now, let us consider how the spin structure evolves upon Co doping. In Fig. 5 we show schematically probable spin configurations on ten (Cu,Co) sites along the chains (a_1-axis) for each doping state. For clarity, the O atoms are omitted. With increasing x, the spin configurations might vary from (a) to (d) at low temperatures, if we could assume that all the spins tend to align parallel to the magnetization easy axis of b-axis. As described above, the non-doped compound $Ca_{0.83}[Cu^{2+}_{0.66}Cu^{3+}_{0.34}]O_2$ is most extensively studied and the Cu^{2+} spins ($S = 1/2$: small arrows) and the Cu^{3+} holes (small open circles: Zhang–Rice singlets [14]) are thought to be distributed as (a) [8,12]. Most of the Cu^{2+} spins are dimerized at lower temperature to form spin–singlet pairs (large ellipses) separated by one Zhang–Rice singlet sites. When one Cu^{3+} hole is

replaced by the Co^{3+} spin ($S = 2$:large arrow), the spin configuration would change as (b). In this state, the short-range magnetic order still survives at some points. With further doping of Co^{3+}, most of the spins align to the *b*-axis as (c). In fact, the 3D AF state appears between the states (b) and (c). At the solubility limit of Co^{3+}, all the spins align to form a ferromagnetic chain (d). This spin arrangement is quite similar to that of the structure analogue $(Ca_{0.565}Y_{0.435})_{0.82}Cu^{2+}O_2$, where all the spins are equivalent and the ferromagnetic chains alternate in an antiparallel manner along the *c*-axis [19]. However, the observed $\chi(T)$ behavior below T_N for the powdered samples is much different between the present Co-doped compound and the Y-doped one: only a few part of the magnetic moment contribute to the 3D magnetic order for the present compound. Similar $\chi(T)$ behavior is frequently observed for a compound which possesses a sine-wave-like modulated spin configuration, such as $PrNi_2Ge_2$ [20]. It is more likely that the present compound also has a similar sine-wave-like spin structure as shown in Fig. 5(e).

Based on the Kanamori mechanism [21], the 90° superexchange interaction between the nearest Cu^{2+} spins mediated by an O^{2-} ion is ferromagnetic (F). On the other hand, those between the nearest Cu^{2+} and Co^{3+} could be either F or AF depending on the hybridization between the doubly degenerated $Co^{3+}(d_{xz}, d_{yz})$ orbitals and the O^{2-} $2p_\pi$ or $2p_\sigma$ orbitals. As shown in Table 2, the observed negative θ values indicate the nearest spins in the present samples are dominated by the AF interaction for the samples with $x \geqslant 0.10$. In similar compounds $(Ca_{0.565}Y_{0.435})_{0.82}Cu^{2+}O_2$ and Li_2CuO_2 [22], powdered samples show negative θ values but the arrangements of the Cu^{2+} spins are ferromagnetic. These facts imply that the second- and further nearest exchange interactions should be important to dictate the spin structures for such compounds. Furthermore, as demonstrated by Mizuno et al., [23], the orthogonal Cu(Co)−O−Cu(Co) angle is also crucial for the exchange interactions, particularly around 95°, where the interaction changes from F to AF. Since the present compound belongs to a composite crystal, the orthogonal Cu(Co)−O−Cu(Co) angle would vary site-by-site due to the displacive modulations of the Cu(Co) and O atoms. Under such a complicated situation, the amplitude-modulated spin structure proposed in Fig. 5(e) could be plausible for the heavily Co-doped region.

In the present solid solution, $Ca_{0.83}$ $(Cu_{1-x}Co_x)O_2$, the formal valence state of the magnetic site is fixed at 2.34 and only the spin quantum number is allowed to change. This is a case complementary to that of another solid solution $(Ca_{1-x}Y_x)_yCuO_2$, in which every equivalent $S = 1/2$ spin can be suitably separated into hole and spins with the change in x. Both the solid solutions are linked with a terminal compound $Ca_{0.83}CuO_2$, where the Zhang–Rice singlets are distributed almost every third magnetic sites. Viewing from this situation, both the phases can be regarded as a solid solution in which the Zhang–Rice singlets are replaced either with $S = 1/2$ spins for the Y-doped case or with $S = 2$ spins for the present Co-doped case. At a certain doping level, both sets of the solid solutions exhibit a magnetic transition from short-range to 3D but the evolution of the spin configuration are considered to be much different. For the complete understanding of the spin structure as well as the modulated structure of the solid solution, low- temperature neutron diffraction study is currently underway.

4. Summary

Partial substitution of the Co ions for the Cu ions in the solid solution $Ca_{0.83}(Cu_{1-x}Co_x)O_2$ $(0 \leqslant x \leqslant 0.30)$ is found to cause both structural change and magnetic phase transition with increasing x. A monoclinic to orthorhombic $(M-O)$ phase change takes place at $x \sim 0.04$ for the $[(Cu, Co)O_2]$ subsystem while such a change occurs at $x \sim 0.17$ for the [Ca] subsystem at room temperature. The doped Co ions are considered to be at a high-spin $(S = 2)$ trivalent state and mainly substitute for the low-spin $(S = 0)Cu^{3+}$ ions in a statistical manner so as to dilute 1D AF interaction and to emerge a long-range AF order with $x \geqslant 0.15$ at lower temperature. As well as the Y-doped analogue, the present compound system could be a good example for studying a doping effect of the magnetic impurity on low-dimensional spin systems.

References

[1] T. Siegrist, R.S. Roth, C.J. Rawn, J.J. Ritter, Chem. Mater. 2 (1990) 192.
[2] T.G.N. Babu, C. Greaves, Matter Res. Bull. 26 (1991) 499.
[3] O. Milat, G. Tendeloo, S. Amelinckx, T.G.N. Babu, C. Greaves, J. Solid State Chem. 97 (1992) 405.
[4] Y. Miyazaki, I. Gameson, P.P. Edwards, J. Solid State Chem. 145 (1999) 511.
[5] Y. Miyazaki, M. Onoda, A. Yamamoto, P.P. Edwards, T. Kajitani, J. Phys. Soc. Jpn. 70 (Suppl. A) (2001) 238.
[6] Y. Miyazaki, M. Onoda, P.P. Edwards, S. Shamoto, T. Kajitani, J. Solid State Chem. 163 (2002) 540.
[7] J. Dolinsek, D. Arcon, P. Cevc, O. Milat, M. Miljak, I. Aviani, Phys. Rev. B 57 (1998) 7798.
[8] M. Isobe, K. Kimoto, E.T. Muromachi, J. Phys. Soc. Jpn. 71 (2002) 782.
[9] G.I. Meijar, C. Rossel, E.M. Kopnin, M. Willemin, J. Karpinski, H. Schwer, K. Conder, P. Wachter, Europhys. Lett. 42 (1998) 339.
[10] A. Hayashi, B. Batlogg, R.J. Cava, Phys. Rev. B 58 (1998) 2678.
[11] Y. Miyazaki, N.C. Hyatt, M. Slaski, I. Gameson, P.P. Edwards, Chem. Eur. J. 5 (1999) 2265.

[12] Z. Hiroi, M. Okumura, T. Yamada, M. Takano, J. Phys. Soc. Jpn. 69 (2000) 1824.
[13] Y. Miyazaki, P.A Anderson, P.P. Edwards, J. Magn. Magn. Mater. 234 (2001) 241.
[14] F.C. Zhang, T.M. Rice, Phys. Rev. B 37 (1988) 3759.
[15] E.T. Muromachi, Y. Uchida, K. Kato, Jpn. J. Appl. Phys. 26 (1987) L2087.
[16] M. Uehara, M. Ogawa, J. Akimitsu, Physica C 255 (1995) 193.
[17] A. Yamamoto, Acta Crystallogr. A 49 (1993) 831.
[18] R.L. Carter, in: Molecular Symmetry and Group Theory, Wiley, New York, 1997.
[19] M. Matsuda, K. Ohoyama, M. Ohashi, J. Phys. Soc. Jpn. 68 (1999) 269.
[20] R. Welter, G. Venturini, B. Malaman, J. Alloys Compd. 329 (2001) 69.
[21] J. Kanamori, J. Phys. Chem. Solids 10 (1959) 87.
[22] N. Boehm, S. Coad, B. Roessli, A. Zheludev, M. Zolliker, P. Boni, D. McK. Paul, H. Eisaki, N. Motoyama, S. Uchida, Europhys. Lett. 43 (1998) 77.
[23] Y. Mizuno, T. Tohyama, S. Maekawa, T. Osafune, N. Motoyama, H. Eisaki, S. Uchida, Phys. Rev. B 57 (1998) 5326.